

L4P: Low-Level 4D Vision Perception Unified

Abhishek Badki* Hang Su* Bowen Wen Orazio Gallo



<https://research.nvidia.com/labs/lpr/l4p>

Abstract

The spatio-temporal relationship between the pixels of a video carries critical information for low-level 4D perception. A single model that reasons about it should be able to solve several such tasks well. Yet, most state-of-the-art methods rely on architectures specialized for the task at hand. We present L4P (pronounced “LAP”), a feedforward, general-purpose architecture that solves low-level 4D perception tasks in a unified framework. L4P combines a ViT-based backbone with per-task heads that are lightweight and therefore do not require extensive training. Despite its general and feedforward formulation, our method matches or surpasses the performance of existing specialized methods on both dense tasks, such as depth or optical flow estimation, and sparse tasks, such as 2D/3D tracking. Moreover, it solves all those tasks at once in a time comparable to that of individual single-task methods.

1. Introduction

Large collections of videos are our most complete and compact source of priors about the world. Much like text did for large-language models, the corpus of videos we amassed over the years allowed video-language models (VLMs) to produce remarkable zero-shot results on high-level vision tasks such as video captioning, video question answering, and others. However, zero-shot, low-level 3D and 4D vision perception tasks, such as depth from video, tracking, optical flow, and others remain a challenge. Pretrained video diffusion models fine-tuned on target-domain data showed potential on dense vision perception tasks (e.g., depth [20, 27], flow [43], etc.), but the fine-tuning makes them task-specific, and therefore limits their ability to leverage priors across multiple tasks at once. Sparse vision perception tasks, such as tracking, are even more challenging to tackle with a general foundation model, because their representation does not fit naturally into data structures like dense

* indicates equal contribution.

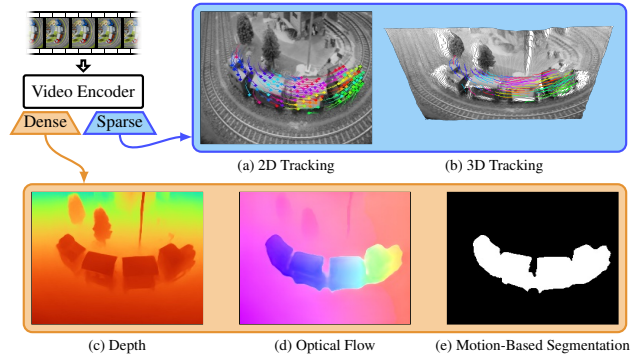


Figure 1. We propose L4P, a single, general-purpose architecture that solves several low-level 4D perception tasks with zero-shot generalization capabilities. We show that a pre-trained video encoder can be combined with lightweight heads and surpass or at least match the performance of SOTA methods, which use specialized architectures and are trained to solve individual tasks.

pixel planes. As a result, they have been historically addressed with carefully designed approaches, which are often optimization-based [59], or with specialized architectures [8, 26].

Can we leverage the priors learned from a large body of video data and solve *multiple* low-level 4D vision perception tasks, both *dense* and *sparse*, with a *unified* architecture, in a *zero-shot* way?

This goal presents multiple challenges. To effectively learn and share priors across tasks—including those beyond 4D perception—we need an architecture with a strong backbone shared across tasks. This architecture should also be general to allow for pretraining on auxiliary tasks. Not least, dense and sparse tasks require fundamentally different representations, e.g., dense 2D planes vs. 3D tracks. We fulfill these requirements by combining a pretrained video masked auto-encoder (VideoMAE) [56, 58] with per-task, lightweight heads (Figure 2). VideoMAEs have been successfully employed for a variety of mid- and high-level vision tasks [58], but their ability to capture the spatio-temporal relationship between pixels is underexplored in the context of low-level 4D perception. We choose a Video-

MAE as the backbone for our system because of the powerful priors it learned in its pretraining. Moreover, VideoMAEs offer a feedforward, online mechanism to tokenize videos within a relatively small computational envelope. For dense tasks, we couple the VideoMAE with heads based on the dense prediction transformer (DPT), which has been shown to perform well on depth estimation, image segmentation, and others [41]. For sparse tasks we focus on tracking, and specifically, on the track-any-point (TAP) formulation [7]. We posit that tracking is important for perception because understanding fine-grained, complex motions and the physical interaction between objects is critical to downstream applications, including 3D reconstruction [32, 57] and robotics manipulation [1, 66, 67, 70]. We formulate the problem of estimating tracks as that of predicting, for queried pixels, 2D heatmaps with associated depth and visibility tokens. This is the mechanism that allows us to tackle sparse and dense tasks within a *unified* framework.

Our formulation presents several desirable properties and advantages. First, the pretrained VideoMAE model allows us to tap into priors learned from large datasets—potentially different and more varied than those typically used for low-level 4D perception. It also affords us efficient computation: our system solves all tasks in roughly 300ms for a 16-frame video chunk ($\sim 19\text{ms}/\text{frame}$), which is comparable to, or faster than, methods specialized for each task (see Table 1 in the Supplementary). Moreover, combining it with per-task heads allows us to train a relatively small number of parameters for new tasks, which we show by freezing the system and adding a head for motion-based segmentation. Lastly, but perhaps most importantly, breaking the architecture into a general VideoMAE and per-task heads offers a mechanism to solve both dense and sparse tasks with a *unified* model (Figure 1). Despite being general, our architecture performs on par with, or better than, state-of-the-art methods. This is remarkable because the baselines we compare against are task-specific, carefully designed for, and specialized to excel at their respective tasks. Finally, VideoMAEs are already used as encoders for VLMs [34, 64], and we speculate that training them to reason about low-level 4D perception may impart those capabilities to the downstream VLMs they may be used with, though validating this statement is outside the scope of our paper.

2. Related Works

Our method unites the strong generalization capabilities of pre-trained foundation models with lightweight task-specific heads. In this section, we review relevant literature for both the foundation models and the individual tasks.

2.1. Foundation models for vision perception

Self-supervised pre-training of large models on huge unlabeled data has shown great success on vision tasks.

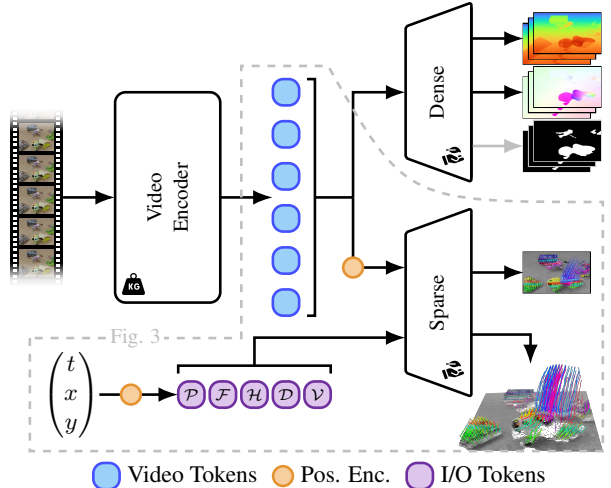


Figure 2. We split our architecture into a powerful encoder, which extracts tokens from the input video, and per-task lightweight heads. For sparse tasks, such as 3D tracking, we define additional query tokens, namely the point we wish to track, \mathcal{P} , with the corresponding feature token, \mathcal{F} , and output tokens (heatmap \mathcal{H} , depth \mathcal{D} , and visibility \mathcal{V}). Figure 3 further details the processing performed by the sparse task head.

Among them, Vision Transformers (ViT) [29] pretrained with masked autoencoding (MAE) [19] have become a major choice to fine-tune for many vision tasks, SegmentAnything (SAM) [28] being a notable example. VideoMAE [56] and MAE-ST [12] adopt MAE on videos for spatio-temporal representation learning. VideoMAEv2 [58] introduces a dual masking strategy that allows them to efficiently scale up the model to a billion parameters and to effectively leverage priors from large data. Their representation shows strong performance on action recognition, and more recently is combined with large language models to enable multimodal video understanding [34, 64]. However, their uses remain unexplored for the low-level 4D perception tasks, which we address in this work.

2.2. Dense Prediction Tasks

We review related works for the dense prediction tasks of depth, flow and motion-based segmentation.

Depth Estimation. Depth perception is critical to many applications, and depending on the use cases many solutions exist for this task. Traditional stereo approaches [14, 15, 46], as well as their more recent deep learning counterparts [21, 44, 75], take two or more posed input views and leverage the underlying 3D correspondences, which limit their uses to only static scenes. Depth estimation from a single image [11, 40, 41, 73, 74] has made impressive progress, but still suffer from 3D and temporal inconsistency, limiting their utility for video settings. In this work, we focus on video depth estimation, which, unlike multi-view

stereo (MVS), focuses on dynamic scenes and assumes no provided camera poses. Some early works rely on test-time optimization [30, 35] to enforce consistency. More recent works introduce feedforward [52, 63] and diffusion-based [20, 48, 76] solutions.

Since depth annotations are limited, many approaches exploiting learned priors from foundation models. DI-NOv2 [38] pretraining allows them to achieve competitive single-image depth estimation quality with only a lightweight head and minimal fine-tuning. DUS3R [60] and MAST3R [33] show that cross-view completion pretraining [65] can provide strong prior for cross-view reasoning. Diffusion models are another powerful source of priors, where Marigold [27] and DepthCrafter [20] demonstrate impressive detailed outputs in single-image and video depth estimation respectively. Like in previous works, we adopt large-scale pretraining by using a video encoder pre-trained with MAE; however, we solve this task along with other 4D perception tasks in a unified framework.

Optical flow estimation. Though straightforward when posed as a dense prediction task, optical flow traditionally requires specialized architectures leveraging domain knowledge to be competitive [50, 53, 61, 69]. Similar to depth estimation, recent works adopt powerful priors from large-scale pretraining, *e.g.* via diffusion priors [43] or large-scale cross-view completion pretraining [65]. Most related to ours are approaches that take multi-frame inputs [10, 23, 42, 49]. They generally showcase improved accuracy and stability in predictions by leveraging temporal coherence; however they all rely on heavily customized networks, in contrast to ours using only generic architectures.

Motion-based segmentation. Early learning-based approaches rely on combining appearance features and optical flow to solve this task [1, 13, 22, 54, 55]. Recent works extract geometric properties from optical flow before using it to train a binary classification network. For example, MoA-Net [4] compensates for the camera rotation in the optical flow, and RigidMask [72] goes further by extracting optical expansion [71] signal from flow and using single-image depth priors. However, they are prone to noises in the estimated flow and are limited by their two-frame formulation. We show that using priors from our video-based approach, we can achieve good performance by only training a task-specific head for this task.

2.3. Sparse Prediction Tasks

Tracking Any Point (TAP) in a video for long durations is fundamental for understanding complex dynamics of the world and has many applications [1, 6, 32, 57, 67]. Particle Video [18], PIPs [3] and TAP-Net [7] lay the initial foundation by adopting several ideas from optical flow approaches like building cost-maps between query points and image features, iterative estimation of tracks, etc. On the

other hand, OmniMotion [59] optimizes a volumetric representation for each video to solve this task, but its time-consuming nature limits its applicability. TAPIR [8] introduces the idea of coarse-to-fine track estimation with a global temporal refinement strategy and BootsTAPIR [9] further improves it by adopting a self-supervised learning approach. CoTracker [26] proposes to jointly track multiple points to leverage spatial correlations and achieve strong 2D tracking performance while still being an online approach. SpaTracker [68] introduces one of the first feedforward 3D point tracking approaches by using depthmaps from a depth estimator to uplift pixels to 3D and leveraging CoTracker’s tracking formulation to track points in 3D.

Unlike previous approaches that rely on carefully designed, specialized architectures, our solution solves both the 2D and 3D point tracking tasks in a single unified framework shared with other tasks. We share some motivations with Tracking at Any Granularity [17], a concurrent work. While they focus on training a large model from scratch on a large collection of datasets for tracking various types of queries, we focus on leveraging large-scale pre-trained models to solve the point tracking task as one of the many capabilities afforded by our unified framework.

3. Method

We provide an overview of our approach in Figure 2. Our model uses a pre-trained ViT-based video encoder [58] (Section 3.1) to capture spatio-temporal features in an RGB video clip of length T . We use lightweight task-specific heads that decode the video features for low-level 3D/4D perception tasks. For pixel-wise dense tasks like depth, flow, and motion-based segmentation, we design a DPT-based head [41], originally only designed for images, to work with videos (Section 3.2). For the sparse task of tracking any pixel in a video, we take inspiration from the head architecture proposed in SAM [28] (Section 3.3). Given a pixel queried in any frame of the input video, we extend the head, also originally designed to work for images, to decode video tokens into a 2D trajectory, its depth with respect to the camera, and the track visibility in each frame (Section 3.3.1). The VideoMAE architecture extracts video tokens from windows of fixed length T , and cannot process longer sequences. To allow for an online approach, we propose a memory mechanism to track points in arbitrarily long videos (Section 3.3.2).

3.1. Video Masked Auto-Encoders

Motivated by scalable and powerful pre-training methods and architectures, we use the ViT-based video encoder from VideoMAEv2 [58], which was pre-trained using the masked auto-encoding task. The encoder works with videos of size $T \times H \times W$, uses a spatio-temporal patch-size of $t \times h \times w$ and cube embedding [56] to transform an input video into

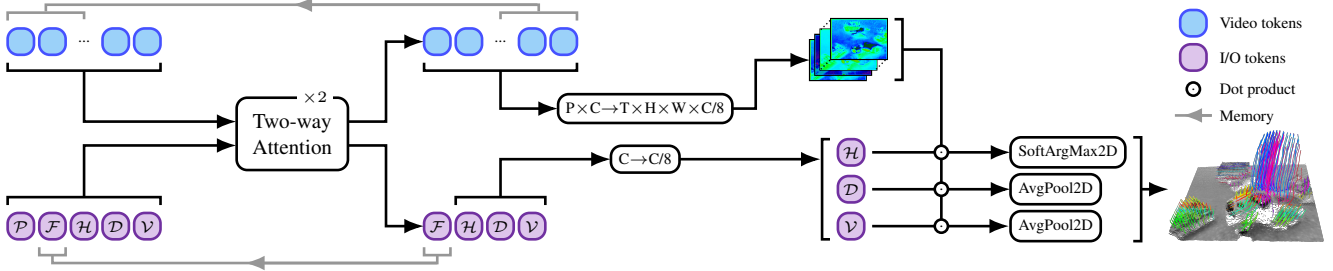


Figure 3. Detailed structure for the sparse head. The tokens extracted from the video and the I/O tokens (query Point token, query point Feature token, and query point Heat map, Depth, and Visibility) tokens are processed by a SAM-style two-way attention layer. The outputs are then reshaped and resized. The resulting per-frame featuremaps and Heat map, Depth, and Visibility tokens are combined via a dot-product. We also implement a memory mechanism that combines the video tokens and the Feature token from overlapping windows.

a sequence of tokens. These are then processed by the ViT architecture with spatio-temporal attention to generate the video tokens $\mathcal{S} \in \mathbb{R}^{P \times C}$, where P is the number of tokens and C is the embedding dimension. We run the video encoder only once per video clip. Once they are encoded, we can apply the lightweight heads to decode the tokens to the desired output. For the point tracking task, we can independently prompt these tokens to track many points in parallel.

3.2. Dense Prediction Heads

Dense prediction tasks produce outputs with spatial dimensions aligned with their inputs, typically at the same resolution $H \times W$. A wide array of common computer vision problems can be formulated as dense prediction tasks. In this work, we explore depth estimation, optical flow estimation, and motion-based segmentation as examples.

It is often critical to capture both local and global spatial structures for dense prediction tasks to succeed. We opt to adapt DPT [41] as our dense prediction head due to its proven performance and efficiency on single-image depth estimation. DPT progressively assembles and combines tokens from various layers inside transformers to produce full-resolution predictions. To leverage the 3D tokens from VideoMAE and to enable temporal reasoning, we replace all 2D convolutions inside the DPT head with 3D convolutions. We find that this modification is enough to bring in temporal consistency with minimal computation overhead. The DPT heads for each of the dense tasks differ only in the final layer, which outputs one channel for depth and motion-based segmentation, and two channels for optical flow.

For videos longer than T frames, we run inference with stride $T/2$. To enforce consistency, we use an affine transformation to align the depth predictions for frames at the overlap of consecutive windows. This strategy has no effect on the individual windows for relative depth, but it greatly improves long-term temporal consistency. For optical flow and motion-based segmentation, we simply overwrite the overlapping predictions.

3.3. Sparse Prediction Heads

Given a pixel prompt, (t_i, x_i, y_i) , in a video, we want to estimate the corresponding 3D trajectory, $\mathcal{T}_i = \{\hat{x}_i(t), \hat{y}_i(t), \hat{d}_i(t), \hat{v}_i(t)\}_{t=0}^{S-1}$, where at time t , $(\hat{x}_i(t), \hat{y}_i(t))$ denotes the 2D track location, $\hat{d}_i(t)$ is the track depth with respect to camera, and $\hat{v}_i(t)$ is the track visibility indicating if a track is visible or occluded. This is a challenging task since it requires tracking the pixel in 2D when visible, tracking it through occlusions, and reasoning about the depth of the track. Moreover, our video encoder has limited temporal context, since it can only process videos with fixed temporal window of T frames, and we want to enable tracking for arbitrarily long videos with $S > T$ frames. This makes adapting a general-purpose head particularly challenging. To tackle this, we adapt an online approach. We propose a head that allows us to estimate the 3D track for an input pixel prompt within the temporal context (T frames) of the video encoder. For online estimation beyond T frames, we propose a memory mechanism for our head and a recipe to train it efficiently (see Figure 3 for an overview).

3.3.1 Tracking within the Temporal Context

Posing the sparse tracking task within our unified framework requires special care. Instead of directly estimating point-track positions, we propose to represent tracks using dense probability heatmaps. Casting tracking as a problem of estimating pixel-aligned 2D maps affords us a shared representation between sparse and dense tasks, which is critical for using a shared backbone. To achieve this, we adapt the prompt-encoding and mask-decoding mechanisms from SAM [28]. The input pixel prompt is encoded using 3D positional encoding and a learnable embedding to generate input point token \mathcal{P} with embedding dimension of C . Similarly, we define output tokens with learnable embeddings to estimate different components of a 3D track: a heatmap token (\mathcal{H}) to estimate the 2D pixel position of the track across

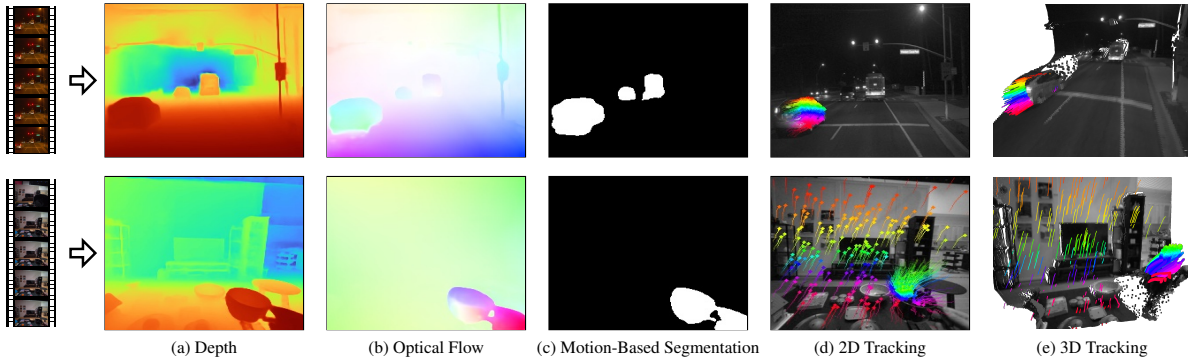


Figure 4. We show results for all perception tasks supported by L4P. Both examples show dynamic scenes with camera and object motions.

the video, a depth (\mathcal{D}) and a visibility (\mathcal{V}) token. Input and output tokens interact with the video tokens, \mathcal{S} , also encoded using 3D positional encoding, using a two-way attention mechanism to decode the video features. These video features are then reshaped and up-sampled, and a final inner product with the processed output tokens gives us output masks of size $T \times H \times W$. For the 2D track estimation, we interpret this output mask as a probability heatmap that encodes the 2D track position and apply a 2D soft-argmax operation to estimate the 2D track position $(\hat{x}_i(t), \hat{y}_i(t))$ at each frame t . For depth and visibility, we simply apply a 2D average pooling operation, followed by exponential and sigmoid operations respectively to estimate the track depth $\hat{d}_i(t)$ and the visibility $\hat{v}_i(t)$ at each frame t . This simple design also allows us to query points anywhere in the video and track them in parallel. We adapt two-way attention from SAM [28] and keep this head lightweight by using only two two-way attention layers. We also replace the 2D convolutions in the original mask-decoder of SAM with 3D convolutions to enable temporal reasoning.

3.3.2 A Memory Mechanism for Long Videos

To track beyond a single window of length T frames, we adopt an online approach.

A naïve approach is to chain tracks across windows. Given two consecutive and overlapping windows, and a 2D track estimated in the first one, we can use a point on the track in the temporal overlap between the two windows as the query for tracking in the second one. To pick a good point to chain the tracks, we can select the one with highest visibility score. However, this solution is brittle. First, a tracked point may not be visible in the overlap between the windows. To tackle this problem, inspired by Karaev *et al.* [26], we introduce a track-feature token \mathcal{F} that is passed to subsequent windows as an additional prompt (see Figure 3). However, unlike Karaev *et al.*, we do not initialize it explicitly with the local appearance around the query point, so the two-way attention head is free to capture the

most useful information to track through occlusions. Second, the naïve solution described above does not allow the system to reason across temporal windows, which makes it prone to drifting or to losing tracks. The track-feature tokens help, but to provide even more cross-window information, we pass the video tokens decoded by the two-way attention stage of the current window to the next, as shown in Figure 3. We achieve this by projecting the decoded video tokens in the overlapping region via a linear layer, and by adding them to the corresponding incoming video tokens to the two-way attention stage in the next window. Our memory strategy based on these two mechanisms is critical to allow proper reasoning across temporal windows as shown by the comparison in ablation study in Section 4.5.

Online training. Training the memory mechanism requires unrolled-window training [26], in which we compute the video features for all the overlapping windows in a video of length S , and then compute the tracks for the entire video in an online fashion. However, training such an approach end-to-end is prohibitive due to memory constraints. To alleviate this, we adapt a two-stage training strategy. First, we train only for a single window but train all the parameters of our network, and in a second stage we freeze all but the last few layers of our video encoder, and fine-tune it along with the tracking head for unrolled window training. In Tables 3 and 4 we show this approach improves the performance over the naïve chaining approach.

4. Experiments

First, we provide details about our architecture and training. Then, for each task, we discuss the baselines, the evaluation metrics and datasets, and show quantitative and qualitative results. We also present an ablation study that evaluates the contribution of different components of our approach. Finally, we show a way to extend our approach to new tasks by using motion-based segmentation as an example.

4.1. Implementation

Training datasets. We use the video encoder from Wang *et al.* [58], which is pre-trained on 1.35M video clips for masked auto-encoding. To fine-tune our model, we use a limited number of synthetic datasets covering a varying range of types of annotations, and rely on the priors from the pre-trained video encoder for generalization. We use Kubric [16], a synthetic dataset in which multiple objects interact, annotated with depth, flow, and 2D and 3D point tracking. To include videos with long 3D trajectories, we add PointOdyssey [77] and DynamicReplica [25]. Both are synthetic datasets with animated characters in mostly indoor scenes. Both datasets have depth annotations and, in addition, DynamicReplica offers optical flow annotations. To further increase scene diversity, we also include TartanAir [62], which provides annotations for flow and depth.

Architectures. Our video encoder [58] processes video-clips of size $16 \times 224 \times 224$. It uses a patch size of $2 \times 14 \times 14$, which results in $P = 2048$ video tokens, and an embedding dimension of $C = 1408$. It has 40 encoder blocks, and we use the output from blocks 14, 21, 28, 36 for DPT heads for dense tasks, while the sparse heads use features only from the last block. Feeding the sparse and dense heads with tokens from different blocks allows us to maintain the performance on dense tasks while we fine-tune our model to train the memory mechanism for the tracking tasks, as we discuss below. For a $16 \times 224 \times 224$ video clip, our method generates the outputs for all our tasks in ~ 300 ms on an NVIDIA A6000 GPU. This corresponds to ~ 19 ms for a single frame, which is competitive with single-task approaches (see Supplementary for detailed comparisons). However, our method’s latency may prevent its use for applications that require strict real-time performance.

Training. We initialize our video encoder using a pre-trained VideoMAE [58] and fine-tune our model in two stages. In both stages, we construct a batch of many tracks per video for the tracking task. In the first stage, we train end-to-end for depth, flow, 2D and 3D point tracking tasks on a single window of $T = 16$ frames. In the second stage, we further fine-tune our model for the tracking tasks using unrolled-window training and the memory mechanism for online tracking. We train on videos of length $S = 40$ by using 4 overlapping windows of size 16 frames and a stride of 8. Due to memory constraints, in the second stage, we freeze all the parameters, except the last three layers (37-39) of the video encoder and the sparse task head. This allows us to maintain the performance on depth and flow, while training the memory mechanism to improve the tracking tasks. Both stages use a batch size of 8 and are trained on a single 8-GPU (NVIDIA A100) node for 100k iterations. Training takes 1 day and 2 days respectively.

Losses. We use the SILog [11] loss for depth and L1 loss for optical flow. For tracking, we use L1 loss for 2D track

	Sintel (~50 frames)		ScanNet (90 frames)		KITTI (~110 frames)		Bonn (110 frames)		NYUv2 (1 frame)	
	AbsRel ↓	δ_1 ↑	AbsRel ↓	δ_1 ↑	AbsRel ↓	δ_1 ↑	AbsRel ↓	δ_1 ↑	AbsRel ↓	δ_1 ↑
Marigold [27]	0.532	0.515	0.166	0.769	0.149	0.796	0.091	0.931	0.070	0.946
DA [73]	0.325	0.564	0.130	0.838	0.142	0.803	0.078	0.939	0.042	0.981
DA-V2 [74]	0.367	0.554	0.135	0.822	0.140	0.804	0.106	0.921	<u>0.043</u>	<u>0.978</u>
NVDS [63]	0.408	0.483	0.187	0.677	0.253	0.588	0.167	0.766	0.151	0.780
ChronoDepth [48]	0.587	0.486	0.159	0.783	0.167	0.759	0.100	0.911	0.073	0.941
DepthCrafter [20]	0.270	0.697	0.123	0.856	0.104	0.896	0.071	<u>0.972</u>	0.072	0.948
L4P-depth (Ours)	<u>0.251</u>	0.659	0.102	0.895	0.099	0.916	0.061	<u>0.972</u>	0.078	0.932
L4P-depth* (Ours)	0.267	<u>0.693</u>	0.070	0.954	0.097	0.903	0.057	<u>0.972</u>	0.078	0.932
L4P (Ours)	0.263	0.662	0.103	0.898	<u>0.093</u>	<u>0.924</u>	0.060	0.973	0.081	0.925
L4P* (Ours)	0.247	0.691	<u>0.072</u>	<u>0.951</u>	0.090	0.928	<u>0.058</u>	0.973	0.081	0.925

Table 1. **Zero-shot depth estimation results.** We compare our methods against both single-image baselines (Row 1-3) and SOTA video depth estimation approaches (Row 4-6). L4P-depth refers to our model trained specifically for depth estimation and L4P refers to the version trained jointly for all tasks. Models marked * have predictions in overlapping windows aligned using the strategy described in Section 3.2. On video datasets (all except NYUv2), our model consistently performs better than DepthCrafter, the closest competition, and by a large margin on ScanNet and KITTI. **Best** and **second best** results are highlighted.

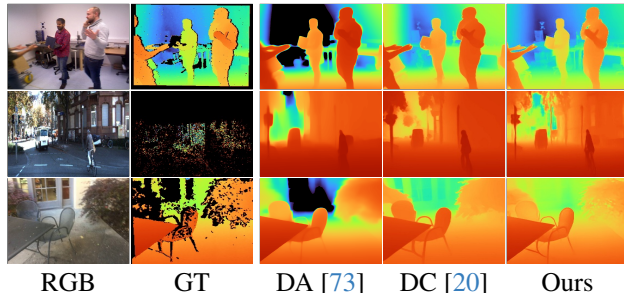


Figure 5. **Qualitative results for depth estimation.** We include one example each from Bonn, KITTI, and ScanNet. Inference is conducted on 16-frame clips, but only 1 frame is shown.

positions, scale-invariant loss for track depth (similar to dense depth), and binary cross entropy loss for track visibility. Like with the choices of tasks heads, we pick the most widely used losses for each of our tasks. However, since we train for multiple tasks at once, weighting the losses appropriately is critical. We find the loss weights empirically by first bringing the losses in the same order of magnitude and then doing a small hyperparameter search around those weights.

Please refer to the Supplementary for additional implementation details.

4.2. Video Depth Estimation

We follow DepthCrafter [20] and evaluate video depth estimation on a collection of five datasets. We do not use any of the datasets for training our models or the baselines to better understand their generalization abilities. There is an inherent scale-ambiguity in the estimated depthmaps. We follow the common practice of aligning linearly the estimation with the GT before calculating evaluation metrics. The alignment is done for all the frames at once, and is carried out in *disparity* space via least-square fitting. For compari-

	Kubric		Dynamic Replica		Spring	
	EPE ↓	EPE < 1 ↑	EPE ↓	EPE < 1 ↑	EPE ↓	EPE < 1 ↑
RAFT* [53]	0.31	94.6	0.14	98.7	0.13	98.4
MemFlow [10]	0.27	95.6	0.11	99.2	0.13	98.4
Ours	(0.13)	(97.6)	(0.03)	(99.9)	0.10	98.5

Table 2. **Optical flow estimation results.** We evaluate on validation sets of all datasets. Our model has seen Kubric and Dynamic Replica during training (numbers in brackets). All others show cross-dataset generalization. On Spring, we surpass both two-frame (marked with *) and multi-frame SOTA baselines, despite the latter having specially designed architectures and a complex memory mechanism.

son on single image datasets, we repeat the single frame 16 times to compute our estimations. We report two metrics: AbsRel (mean($|\hat{\mathbf{d}} - \mathbf{d}|/\mathbf{d}$)) and δ_1 (ratio of pixels satisfying $\max(\mathbf{d}/\hat{\mathbf{d}}, \hat{\mathbf{d}}/\mathbf{d}) < 1.25$), where \mathbf{d} represents GT, and $\hat{\mathbf{d}}$ is depth estimation after alignment. We upsample our estimations from 224×224 to each dataset’s original resolution for evaluation.

We consider video approaches including NVDS [63], ChronoDepth [48], DepthCrafter [20], as well as single-image ones, including Marigold [27] and DepthAnything [73, 74]. Among them, DepthCrafter [20] and DepthAnything [73, 74] each represent the SOTA respectively. Marigold and DepthCrafter are diffusion models, which afford impressive levels of details, but require an expensive iterative denoising process.

Our results show consistent advantages over both SOTA single-image and video depth approaches on the four video datasets (Table 1). Since L4P is a video approach, applying it on single images from NYUv2 does not provide the necessary temporal context for it to perform well. DepthCrafter also similarly suffers on NYUv2. Figure 5 shows qualitative samples and comparison with select SOTA approaches. L4P produces a level of details comparable to that of diffusion models such as DepthCrafter, while generally capturing more accurate relative scales.

Discussion. Our final model performs on par with a specialized depth model (Table 1), despite optimized jointly for all of our tasks. Scale alignment between windows for online inference makes a significant impact on ScanNet. This is due to the fast-paced view change in ScanNet samples making scale inconsistency between windows more prominent. It is also worth noting that L4P performs competitively on KITTI, despite not fine-tuned on synthetic datasets that include driving scenarios.

4.3. Multi-Frame Optical Flow Estimation

We use the Spring dataset [37] for evaluation. We sample 289 16-frame clips from the *train* split. Spring is not used to train ours or other approaches we compare against, allowing us to evaluate generalization ability. The input frames are

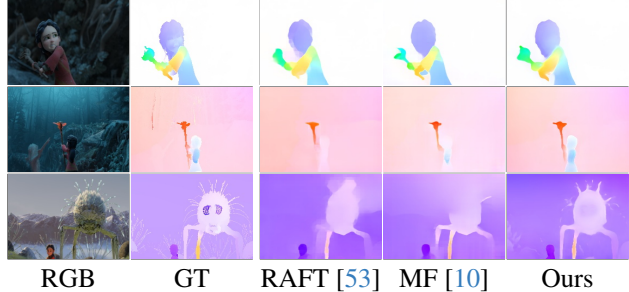


Figure 6. **Qualitative results for optical flow estimation on Spring.** Our results compare favorably to baselines in terms of both details and accuracy. Inference is conducted on 16-frame clips, but only 1 frame is shown.

	Aria	DriveTrack	PStudio	Overall		
	2D-AJ ↑	2D-AJ ↑	2D-AJ ↑	2D-AJ ↑	APD ↑	OA ↑
TAPIR [8]	48.6	57.2	48.7	53.2	67.4	80.5
BootsTAPIR [9]	54.7	62.9	52.4	59.1	74.7	85.6
CoTracker [26]	54.2	59.8	51.0	57.2	74.2	84.5
Ours (2D Only)	56.7	54.2	49.8	53.5	69.4	88.6
Ours (w/o Mem)	36.8	47.4	41.1	41.8	62.9	78.6
Ours	53.0	51.6	48.8	51.2	67.0	88.7

Table 3. **Evaluation of 2D point tracking on TAPVid-3D.** 2D GT trajectories are obtained by projecting 3D GT trajectories onto 2D. Though behind 2D SOTA approaches, our model performs competitively once trained specifically for 2D tracking (“2D Only”).

resized to 224×224 for all evaluation. We use the Endpoint Error (EPE), as well as a more robust metric, ratio of EPE < 1, for the evaluation.

We consider two baselines for comparison. RAFT [53], a competitive and widely used two-frame approach, creates dense pairwise pixel features and uses recurrent updates to estimate optical flow. MemFlow [10], a recently published work, ranks among the top methods on the Spring benchmark. It is a multi-frame approach that relies on a memory mechanism to leverage temporal context. Quantitatively, L4P compares favorably to both RAFT and MemFlow on Spring (Table 2). Our model can capture well both small and large motions and presents more precise motion boundaries (Figure 6). In addition, multi-frame approaches like MemFlow and ours generally have an edge in temporal stability (see Supplementary). Unlike many specialized approaches, our model currently only operates on low-resolution videos and further work is needed to enable efficient high-res estimation.

4.4. Sparse 2D/3D Track Estimation

We evaluate on TAPVid-3D [31], a benchmark containing around 2.1M long-range 3D point trajectories from over 4000 real-world videos, covering a variety of objects, camera and object motion patterns, and indoor and outdoor environments. It consists of three datasets: Aria [39], Drive-

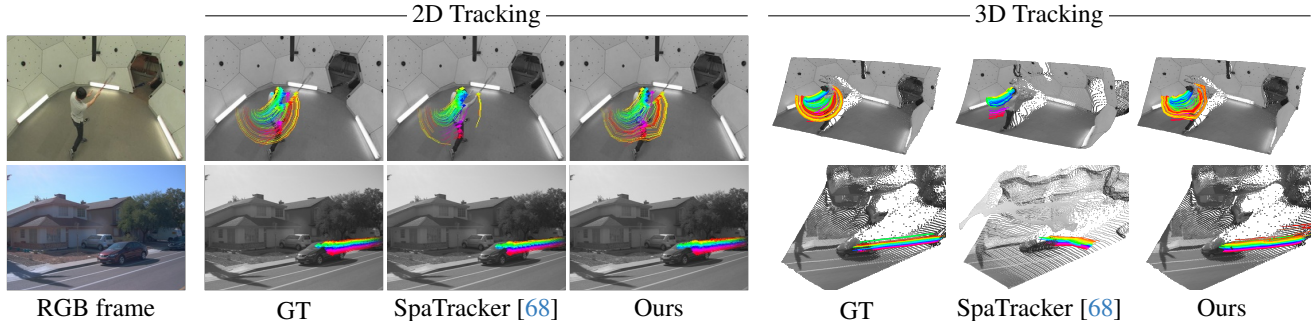


Figure 7. **Qualitative results of Sparse 2D/3D tracking on the TAPVid-3D benchmark.** Comparison with SpaTracker, a SOTA 3D tracking approach, demonstrates the superior quality of our 2D and 3D tracks. For joint visualization of depth and 3D tracks, we align them using median scaling. We use our depth maps for visualization of GT and for SpaTracker we use the ones used by their approach.

	Aria			DriveTrack			PStudio			Overall		
	3D-AJ \uparrow	APD \uparrow	OA \uparrow	3D-AJ \uparrow	APD \uparrow	OA \uparrow	3D-AJ \uparrow	APD \uparrow	OA \uparrow	3D-AJ \uparrow	APD \uparrow	OA \uparrow
Static Baseline	4.9	10.2	55.4	3.9	6.5	80.8	5.9	11.5	75.8	4.9	9.4	70.7
TAPIR + CM	7.1	11.9	72.6	3.9	14.7	80.4	6.1	10.7	75.2	7.4	12.4	76.1
CoTracker + CM	8.0	12.3	78.6	11.7	19.1	81.7	8.1	13.5	77.2	9.3	15.0	79.1
BootsTAPIR + CM	9.1	14.5	78.6	11.8	18.6	83.8	6.9	11.6	81.8	9.3	14.9	81.4
TAPIR + ZD	9.0	14.3	79.7	5.2	8.8	81.6	10.7	18.2	78.7	8.3	13.8	80.0
CoTracker + ZD	10.0	15.9	87.8	5.0	9.1	82.6	11.2	19.4	80.0	8.7	14.8	83.4
BootsTAPIR + ZD	9.9	16.3	86.5	5.4	9.2	85.3	11.3	19.0	82.7	8.8	14.8	84.8
TAPIR-3D	2.5	4.8	86.0	3.2	5.9	83.3	3.6	7.0	78.9	3.1	5.9	82.8
SpatialTracker	9.9	16.1	89.0	6.2	11.1	83.7	10.9	19.2	78.6	9.0	15.5	83.7
Ours (w/o Mem)	8.2	15.4	72.7	5.5	10.0	83.3	15.1	25.2	79.9	9.6	16.9	78.6
Ours	11.2	17.7	90.3	6.6	11.4	88.1	18.6	28.2	87.6	12.1	19.1	88.7

Table 4. **Evaluation of 3D tracking on the *full_eval* split of TAPVid-3D.** The top approaches combine 2D point tracking approaches with COLMAP (CM) [45], while the bottom ones, including ours are feedforward. Our approach consistently outperforms previous feedforward works, and also COLMAP baselines on average. We also show the impact of our memory mechanism (Ours vs. Ours w/o Mem). “ZD” refers to ZoeDepth.

eTrack [51], and PStudio [24]. It introduced several baselines by combining SOTA 2D point tracking approaches, such as TAPIR [8], BootsTAPIR [9], and CoTracker [26], with depth solutions like ZoeDepth [2], a monocular depth estimation approach, and COLMAP [45, 47], a structure-from-motion pipeline. The top performing approach on the benchmark is SpaTracker [68].

The benchmark evaluates both 3D and 2D tracking approaches, and uses metrics that measure the ability to predict point visibility using an occlusion accuracy metric (OA), the accuracy of predicted trajectories in the visible regions (APD), and joint occlusion and geometric estimation (AJ). To resolve the scale ambiguity in depth estimation, the benchmark uses global median scaling by computing the median of the depth ratios between the estimated and ground-truth 3D tracks over all the points and frames in a video. We use the *full_eval* split evaluation numbers provided in the TAPVid-3D benchmark for comparing approaches.

On 3D tracking, we outperform previous approaches on average across all the metrics (Table 4). Among feedforward approaches, we perform better on all the datasets. Ap-

proaches that combine 2D track estimation with COLMAP perform better on the DriveTrack [51] dataset. This could be due to a relatively large bias of tracking mostly static vehicles, where COLMAP gives much more accurate depth. Such COLMAP-based baselines, however, perform poorly on Aria [39] and PStudio [24], which are mostly dynamic. We show qualitative evaluation against the SOTA SpaTracker approach in Figure 7.

On 2D tracking, we are slightly behind the SOTA 2D tracking approaches (Table 3). Our approach becomes more competitive and performs better than TAPIR on average when we fine-tune our model only for the 2D tracking task. We believe our reduced performance on 2D tracking comes from working at lower image resolution, 224×224 for us as compared to 384×512 for CoTracker and 256×256 for others, and a lack of task-specific tricks, like tracking multiple points together (CoTracker) or assuming access to all frames in the video and performing a global track-refinement (TAPIR and BootsTAPIR), both of which could also benefit our tracking head. We also ablate our online tracking approach on both 2D and 3D tracking benchmarks, and show improved performance due to the use of memory mechanism when tracking points from one window to next. Overall, we attribute our strong performance to our unified approach and carefully designed sparse head.

4.5. Ablations

To understand the contribution of different components of our approach, we perform an ablation study for depth, flow, 2D and 3D point tracking, as shown in Table 5. For each of these tasks, we report average over the datasets not used in our training: for depth we use datasets in Table 1, for optical flow we use the Spring dataset, and for tracking we use the *minival* split from the TAPVid-3D [31] benchmark. Our main contribution is to show how to leverage the priors of a pretrained VideoMAE for multiple dense and sparse low-level 4D perception tasks at once. To show the usefulness of our end-to-end fine-tuning strategy, we compare against

	Depth	Optical flow	2D Track	3D Track
	AbsRel \downarrow / $\delta_1 \uparrow$	EPE \downarrow / EPE $< 1 \uparrow$	2D-AJ \uparrow	3D-AJ \uparrow
From scratch	0.259 / 0.594	0.246 / 96.2	16.6	1.3
VideoMAE frozen	0.137 / 0.841	0.120 / 98.2	29.3	3.3
Ours (w/o Mem)	0.120 / 0.876	0.100 / 98.5	41.1	8.7
Ours	0.120 / 0.876	0.100 / 98.5	50.2	10.8

Table 5. **Ablation study.** Training using pre-trained VideoMAE performs better than training from scratch (row 3 vs. 1), which shows our approach leverages VideoMAE priors. Our approach performs better than using a frozen VideoMAE and only fine-tuning the heads (row 3 vs. 2), which shows end-to-end fine-tuning helps. Adding memory mechanism and two-stage training strategy improves tracking performance while maintaining performance on other tasks (row 4 vs. 3).

a pretrained and frozen VideoMAE, where we only fine-tune the task-specific heads. Table 5 shows that our fine-tuned VideoMAE (row 3) produces better results than the pretrained and frozen VideoMAE across all tasks (row 2). A version trained end-to-end from scratch results in worse performance (row 1), which shows that our system leverages the pretraining of the VideoMAE. Finally, by adding the proposed memory mechanism for the tracking head and using our two-stage training process, we obtain improvements in both 2D and 3D tracking tasks, while maintaining the performance on other tasks.

4.6. Additional Task: Motion-based Segmentation

We use the motion-based segmentation task to show one way to add a new task to our network. We do this simply by freezing our trained video encoder and fine-tuning our proposed dense head for this task. We generate the ground-truth annotations for training and evaluation by using *video* datasets that provide camera, depth and 3D-motion information. For training, we use the Kubric [16] dataset and fine-tune using binary cross entropy loss. For evaluation, we use the Virtual KITTI (VKITTI) [5] and Spring [37] datasets. We compare against RigidMask (RM) [72], a SOTA two-frame rigid-motion segmentation approach that combines dynamic motion signals from flow, optical-expansion [71] and depth. It is trained on the Scene-FlowDatasets [36]; however, they also train a version for driving scenarios (RM-Drive). To evaluate, we report foreground IoU (higher is better) on VKITTI and Spring.

On both datasets, our video-based approach achieves better performance. Note that while fine-tuning on driving scenes allows RigidMask (RM-Drive) to reduce the gap slightly on VKITTI, it significantly hurts performance on Spring, highlighting the benefit of our model’s generalization ability. As shown in Figure 8, for both the indoor scenarios with human-object interactions and the outdoor driving scenarios, our approach performs better and can detect small motions (see more comparisons in Supplementary). Freezing the video encoder and fine-tuning a

	VKITTI	Spring
RM	32.6	16.5
RM-Drive	35.4	8.5
Ours	46.7	23.7

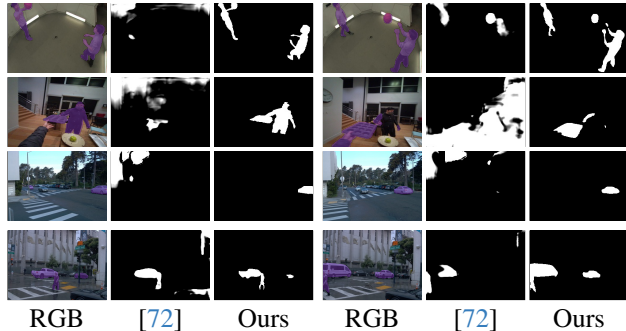


Figure 8. **Qualitative results of motion-based segmentation.** Samples are chosen from the TAPVid-3D benchmark. Across various scenarios, ours show advantages in small motions, boundary accuracy, as well as temporal consistency (see Supp.). The GT masks overlaid on images are only provided to identify qualitatively which objects are moving, but are not pixel-accurate.

task-specific head is the simplest way to add a new task that does not affect the performance of other tasks we train for. Better strategies may exist that allow for some fine-tuning of the video encoder without affecting the performance of other tasks, though the investigation is outside the scope of this paper.

5. Conclusions

We present a unified framework to solve multiple low-level 4D vision perception tasks, both dense and sparse. We achieve this by adopting a strong pre-trained video masked auto-encoder and design lightweight task heads to harness its representation power. Our simple yet versatile designs for task heads allows for effortless and generalizable adaptation to multiple 4D vision perception tasks.

6. Acknowledgements

We would like to thank Jan Kautz for the continuous discussions and for reviewing an early draft of the paper, Zhiding Yu and Hongxu (Danny) Yin for the initial discussions on video models, and Yiqing Liang for help with the data.

References

- [1] Homanga Bharadhwaj, Roozbeh Mottaghi, Abhinav Gupta, and Shubham Tulsiani. Track2act: Predicting point tracks from internet videos enables generalizable robot manipulation. In *European Conference on Computer Vision (ECCV)*, 2024. 2, 3
- [2] Shariq Farooq Bhat, Reiner Birkel, Diana Wofk, Peter Wonka, and Matthias Müller. ZoeDepth: Zero-shot transfer by combining relative and metric depth. *ArXiv Preprint*, 2023. 8
- [3] Weikang BIAN, Zhaoyang Huang, Xiaoyu Shi, Yitong Dong, Yijin Li, and Hongsheng Li. Context-PIPs: Persistent independent particles demands context features. In *Advances*

- in *Neural Information Processing Systems (NeurIPS)*, 2023. 3
- [4] Pia Bideau, Rakesh R. Menon, and Erik Learned-Miller. MoA-Net: Self-supervised motion segmentation. In *ECCV 2018 Workshops*, 2019. 3
- [5] Yohann Cabon, Naila Murray, and Martin Humenberger. Virtual KITTI 2. *ArXiv Preprint*, 2020. 9
- [6] Yangming Cheng, Liulei Li, Yuanyou Xu, Xiaodi Li, Zongxin Yang, Wenguan Wang, and Yi Yang. Segment and track anything. *ArXiv Preprint*, 2023. 3
- [7] Carl Doersch, Ankush Gupta, Larisa Markeeva, Adria Recasens, Lucas Smaira, Yusuf Aytar, João Carreira, Andrew Zisserman, and Yi Yang. TAP-Vid: A benchmark for tracking any point in a video. *Advances in Neural Information Processing Systems (NeurIPS)*, 2022. 2, 3
- [8] Carl Doersch, Yi Yang, Mel Vecerik, Dilara Gokay, Ankush Gupta, Yusuf Aytar, Joao Carreira, and Andrew Zisserman. TAPIR: Tracking any point with per-frame initialization and temporal refinement. In *IEEE International Conference on Computer Vision (ICCV)*, 2023. 1, 3, 7, 8
- [9] Carl Doersch, Yi Yang, Dilara Gokay, Pauline Luc, Skanda Koppula, Ankush Gupta, Joseph Heyward, Ross Goroshin, João Carreira, and Andrew Zisserman. BootsTAP: Bootstrapped training for tracking-any-point. *ArXiv Preprint*, 2024. 3, 7, 8
- [10] Qiaole Dong and Yanwei Fu. MemFlow: Optical flow estimation and prediction with memory. In *IEEE Conference on Computer Vision and Pattern Recognition (CVPR)*, 2024. 3, 7, 1
- [11] David Eigen, Christian Puhersch, and Rob Fergus. Depth map prediction from a single image using a multi-scale deep network. *Advances in neural information processing systems*, 27, 2014. 2, 6
- [12] Christoph Feichtenhofer, Haoqi Fan, Yanghao Li, and Kaiming He. Masked autoencoders as spatiotemporal learners. In *Advances in Neural Information Processing Systems (NeurIPS)*, 2022. 2
- [13] Katerina Fragkiadaki, Pablo Arbelaez, Panna Felsen, and Jitendra Malik. Learning to segment moving objects in videos. In *IEEE Conference on Computer Vision and Pattern Recognition (CVPR)*, 2015. 3
- [14] Yasutaka Furukawa and Jean Ponce. Accurate, dense, and robust multiview stereopsis. *IEEE transactions on pattern analysis and machine intelligence*, 32(8):1362–1376, 2009. 2
- [15] Silvano Galliani, Katrin Lasinger, and Konrad Schindler. Massively parallel multiview stereopsis by surface normal diffusion. In *Proceedings of the IEEE international conference on computer vision*, pages 873–881, 2015. 2
- [16] Klaus Greff, Francois Belletti, Lucas Beyer, Carl Doersch, Yilun Du, Daniel Duckworth, David J Fleet, Dan Gnanaprasam, Florian Golemo, Charles Herrmann, et al. Kubric: A scalable dataset generator. In *IEEE Conference on Computer Vision and Pattern Recognition (CVPR)*, 2022. 6, 9, 1
- [17] Adam Harley, Yang You, Yang Zheng, Xinglong Sun, Nikhil Raghuraman, Sheldon Liang, Wen-Hsuan Chu, Suya You, Achal Dave, Pavel Tokmakov, Rares Ambrus, Katerina Fragkiadaki, and Leonidas Guibas. TAG: Tracking at any granularity. In *ArXiv Preprint*, 2024. 3
- [18] Adam W. Harley, Zhaoyuan Fang, and Katerina Fragkiadaki. Particle video revisited: Tracking through occlusions using point trajectories. In *European Conference on Computer Vision (ECCV)*, 2022. 3
- [19] Kaiming He, Xinlei Chen, Saining Xie, Yanghao Li, Piotr Dollár, and Ross Girshick. Masked autoencoders are scalable vision learners. In *Proceedings of the IEEE/CVF conference on computer vision and pattern recognition*, pages 16000–16009, 2022. 2
- [20] Wenbo Hu, Xiangjun Gao, Xiaoyu Li, Sijie Zhao, Xi-aodong Cun, Yong Zhang, Long Quan, and Ying Shan. DepthCrafter: Generating consistent long depth sequences for open-world videos. *ArXiv Preprint*, 2024. 1, 3, 6, 7
- [21] Po-Han Huang, Kevin Matzen, Johannes Kopf, Narendra Ahuja, and Jia-Bin Huang. Deepmvs: Learning multi-view stereopsis. In *Proceedings of the IEEE conference on computer vision and pattern recognition*, pages 2821–2830, 2018. 2
- [22] Suyog Jain, Bo Xiong, and Kristen Grauman. FusionSeg: Learning to combine motion and appearance for fully automatic segmentation of generic objects in videos. *ArXiv Preprint*, 2017. 3
- [23] Joel Janai, Fatma Guney, Anurag Ranjan, Michael Black, and Andreas Geiger. Unsupervised learning of multi-frame optical flow with occlusions. In *Proceedings of the European conference on computer vision (ECCV)*, pages 690–706, 2018. 3
- [24] Hanbyul Joo, Hao Liu, Lei Tan, Lin Gui, Bart Nabbe, Iain Matthews, Takeo Kanade, Shohei Nobuhara, and Yaser Sheikh. Panoptic Studio: A massively multiview system for social motion capture. In *IEEE International Conference on Computer Vision (ICCV)*, 2015. 8
- [25] Nikita Karaev, Ignacio Rocco, Benjamin Graham, Natalia Neverova, Andrea Vedaldi, and Christian Rupprecht. DynamicStereo: Consistent dynamic depth from stereo videos. In *IEEE Conference on Computer Vision and Pattern Recognition (CVPR)*, 2023. 6, 1
- [26] Nikita Karaev, Ignacio Rocco, Benjamin Graham, Natalia Neverova, Andrea Vedaldi, and Christian Rupprecht. Co-Tracker: It is better to track together. In *European Conference on Computer Vision (ECCV)*, 2024. 1, 3, 5, 7, 8
- [27] Bingxin Ke, Anton Obukhov, Shengyu Huang, Nando Metzger, Rodrigo Caye Daudt, and Konrad Schindler. Repurposing diffusion-based image generators for monocular depth estimation. In *Proceedings of the IEEE/CVF Conference on Computer Vision and Pattern Recognition*, pages 9492–9502, 2024. 1, 3, 6, 7
- [28] Alexander Kirillov, Eric Mintun, Nikhila Ravi, Hanzi Mao, Chloe Rolland, Laura Gustafson, Tete Xiao, Spencer Whitehead, Alexander C. Berg, Wan-Yen Lo, et al. Segment anything. In *IEEE International Conference on Computer Vision (ICCV)*, 2023. 2, 3, 4, 5, 1
- [29] Alexander Kolesnikov, Alexey Dosovitskiy, Dirk Weissenborn, Georg Heigold, Jakob Uszkoreit, Lucas Beyer, Matthias Minderer, Mostafa Dehghani, Neil Houlsby, Syl-

- vain Gelly, Thomas Unterthiner, and Xiaohua Zhai. An image is worth 16x16 words: Transformers for image recognition at scale. In *International Conference on Learning Representations (ICLR)*, 2021. 2
- [30] Johannes Kopf, Xuejian Rong, and Jia-Bin Huang. Robust consistent video depth estimation. In *Proceedings of the IEEE/CVF Conference on Computer Vision and Pattern Recognition*, pages 1611–1621, 2021. 3
- [31] Skanda Koppula, Ignacio Rocco, Yi Yang, Joe Heyward, João Carreira, Andrew Zisserman, Gabriel Brostow, and Carl Doersch. TAPVid-3D: A benchmark for tracking any point in 3d. *ArXiv Preprint*, 2024. 7, 8
- [32] Jiahui Lei, Yijia Weng, Adam Harley, Leonidas Guibas, and Kostas Daniilidis. MoSca: Dynamic gaussian fusion from casual videos via 4D motion scaffolds. *ArXiv Preprint*, 2024. 2, 3
- [33] Vincent Leroy, Yann Cabon, and Jérôme Revaud. Grounding image matching in 3d with mast3r. *arXiv preprint arXiv:2406.09756*, 2024. 3
- [34] Kunchang Li, Yanan He, Yi Wang, Yizhuo Li, Wenhai Wang, Ping Luo, Yali Wang, Limin Wang, and Yu Qiao. Videochat: Chat-centric video understanding. *ArXiv Preprint*, 2023. 2
- [35] Xuan Luo, Jia-Bin Huang, Richard Szeliski, Kevin Matzen, and Johannes Kopf. Consistent video depth estimation. *ACM Transactions on Graphics (ToG)*, 39(4):71–1, 2020. 3
- [36] N. Mayer, E. Ilg, P. Häusser, P. Fischer, D. Cremers, A. Dosovitskiy, and T. Brox. A large dataset to train convolutional networks for disparity, optical flow, and scene flow estimation. In *IEEE Conference on Computer Vision and Pattern Recognition (CVPR)*, 2016. 9
- [37] Lukas Mehl, Jenny Schmalfluss, Azin Jahedi, Yaroslava Nalivayko, and Andrés Bruhn. Spring: A high-resolution high-detail dataset and benchmark for scene flow, optical flow and stereo. In *Proceedings of the IEEE/CVF Conference on Computer Vision and Pattern Recognition*, pages 4981–4991, 2023. 7, 9
- [38] Maxime Oquab, Timothée Darcet, Théo Moutakanni, Huy Vo, Marc Szafraniec, Vasil Khalidov, Pierre Fernandez, Daniel Haziza, Francisco Massa, Alaaeldin El-Nouby, et al. Dinov2: Learning robust visual features without supervision. *arXiv preprint arXiv:2304.07193*, 2023. 3
- [39] Xiaqing Pan, Nicholas Charron, Yongqian Yang, Scott Peters, Thomas Whelan, Chen Kong, Omkar Parkhi, Richard Newcombe, and Yuheng Carl Ren. Aria digital twin: A new benchmark dataset for egocentric 3D machine perception. In *IEEE Conference on Computer Vision and Pattern Recognition (CVPR)*, 2023. 7, 8
- [40] René Ranftl, Katrin Lasinger, David Hafner, Konrad Schindler, and Vladlen Koltun. Towards robust monocular depth estimation: Mixing datasets for zero-shot cross-dataset transfer. *IEEE Transactions on Pattern Analysis and Machine Intelligence (TPAMI)*, 2020. 2
- [41] René Ranftl, Alexey Bochkovskiy, and Vladlen Koltun. Vision transformers for dense prediction. In *IEEE International Conference on Computer Vision (ICCV)*, 2021. 2, 3, 4, 1
- [42] Zhile Ren, Orazio Gallo, Deqing Sun, Ming-Hsuan Yang, Erik B Sudderth, and Jan Kautz. A fusion approach for multi-frame optical flow estimation. In *2019 IEEE Winter Conference on Applications of Computer Vision (WACV)*, pages 2077–2086. IEEE, 2019. 3
- [43] Saurabh Saxena, Charles Herrmann, Junhwa Hur, Abhishek Kar, Mohammad Norouzi, Deqing Sun, and David J Fleet. The surprising effectiveness of diffusion models for optical flow and monocular depth estimation. *Advances in Neural Information Processing Systems*, 36, 2024. 1, 3
- [44] Mohamed Sayed, John Gibson, Jamie Watson, Victor Prisacariu, Michael Firman, and Clément Godard. Simplerecon: 3d reconstruction without 3d convolutions. In *European Conference on Computer Vision*, pages 1–19. Springer, 2022. 2
- [45] Johannes Lutz Schönberger and Jan-Michael Frahm. Structure-from-motion revisited. In *IEEE Conference on Computer Vision and Pattern Recognition (CVPR)*, 2016. 8
- [46] Johannes L Schönberger, Enliang Zheng, Jan-Michael Frahm, and Marc Pollefeys. Pixelwise view selection for unstructured multi-view stereo. In *Computer Vision—ECCV 2016: 14th European Conference, Amsterdam, The Netherlands, October 11–14, 2016, Proceedings, Part III 14*, pages 501–518. Springer, 2016. 2
- [47] Johannes Lutz Schönberger, Enliang Zheng, Marc Pollefeys, and Jan-Michael Frahm. Pixelwise view selection for unstructured multi-view stereo. In *European Conference on Computer Vision (ECCV)*, 2016. 8
- [48] Jiahao Shao, Yuanbo Yang, Hongyu Zhou, Youmin Zhang, Yujun Shen, Matteo Poggi, and Yiyi Liao. Learning temporally consistent video depth from video diffusion priors. *arXiv preprint arXiv:2406.01493*, 2024. 3, 6, 7
- [49] Xiaoyu Shi, Zhaoyang Huang, Weikang Bian, Dasong Li, Manyuan Zhang, Ka Chun Cheung, Simon See, Hongwei Qin, Jifeng Dai, and Hongsheng Li. VideoFlow: Exploiting temporal cues for multi-frame optical flow estimation. In *Proceedings of the IEEE/CVF International Conference on Computer Vision*, pages 12469–12480, 2023. 3
- [50] Deqing Sun, Xiaodong Yang, Ming-Yu Liu, and Jan Kautz. Pwc-net: Cnns for optical flow using pyramid, warping, and cost volume. In *Proceedings of the IEEE conference on computer vision and pattern recognition*, pages 8934–8943, 2018. 3
- [51] Pei Sun, Henrik Kretzschmar, Xerxes Dotiwalla, Aurélien Chouard, Vijaysai Patnaik, Paul Tsui, James Guo, Yin Zhou, Yuning Chai, Benjamin Caine, Vijay Vasudevan, Wei Han, Jiquan Ngiam, Hang Zhao, Aleksei Timofeev, Scott Ettinger, Maxim Krivokon, Amy Gao, Aditya Joshi, Yu Zhang, Jonathon Shlens, Zhifeng Chen, and Dragomir Anguelov. Scalability in perception for autonomous driving: Waymo open dataset. In *IEEE Conference on Computer Vision and Pattern Recognition (CVPR)*, 2020. 8
- [52] Zachary Teed and Jia Deng. Deepv2d: Video to depth with differentiable structure from motion. *arXiv preprint arXiv:1812.04605*, 2018. 3
- [53] Zachary Teed and Jia Deng. RAFT: Recurrent all-pairs field transforms for optical flow. In *European Conference on Computer Vision (ECCV)*, 2020. 3, 7, 1
- [54] Pavel Tokmakov, Karteek Alahari, and Cordelia Schmid.

- Learning motion patterns in videos. In *IEEE Conference on Computer Vision and Pattern Recognition (CVPR)*, 2017. 3
- [55] Pavel Tokmakov, Karteek Alahari, and Cordelia Schmid. Learning video object segmentation with visual memory. In *IEEE International Conference on Computer Vision (ICCV)*, 2017. 3
- [56] Zhan Tong, Yibing Song, Jue Wang, and Limin Wang. VideoMAE: Masked autoencoders are data-efficient learners for self-supervised video pre-training. In *Advances in Neural Information Processing Systems (NeurIPS)*, 2022. 1, 2, 3
- [57] Jianyuan Wang, Nikita Karaev, Christian Rupprecht, and David Novotny. VGGsFM: Visual geometry grounded deep structure from motion. 2024. 2, 3
- [58] Limin Wang, Bingkun Huang, Zhiyu Zhao, Zhan Tong, Yinan He, Yi Wang, Yali Wang, and Yu Qiao. VideoMAE V2: Scaling video masked autoencoders with dual masking. In *IEEE Conference on Computer Vision and Pattern Recognition (CVPR)*, 2023. 1, 2, 3, 6
- [59] Qianqian Wang, Yen-Yu Chang, Ruojin Cai, Zhengqi Li, Bharath Hariharan, Aleksander Holynski, and Noah Snavely. Tracking everything everywhere all at once. In *IEEE International Conference on Computer Vision (ICCV)*, 2023. 1, 3
- [60] Shuzhe Wang, Vincent Leroy, Yohann Cabon, Boris Chidlovskii, and Jerome Revaud. Dust3r: Geometric 3d vision made easy. In *Proceedings of the IEEE/CVF Conference on Computer Vision and Pattern Recognition*, pages 20697–20709, 2024. 3
- [61] Shizun Wang, Xingyi Yang, Qihong Shen, Zhenxiang Jiang, and Xinchao Wang. Gflow: Recovering 4d world from monocular video. *arXiv preprint arXiv:2405.18426*, 2024. 3
- [62] Wenshan Wang, DeLong Zhu, Xiangwei Wang, Yaoyu Hu, Yuheng Qiu, Chen Wang, Yafei Hu, Ashish Kapoor, and Sebastian Scherer. TartanAir: A dataset to push the limits of visual slam. In *International Conference on Intelligent Robots and Systems (IROS)*, 2020. 6, 1
- [63] Yiran Wang, Min Shi, Jiaqi Li, Zihao Huang, Zhiguo Cao, Jianming Zhang, Ke Xian, and Guosheng Lin. Neural video depth stabilizer. In *Proceedings of the IEEE/CVF International Conference on Computer Vision*, pages 9466–9476, 2023. 3, 6, 7
- [64] Yi Wang, Kunchang Li, Xinhao Li, Jiashuo Yu, Yinan He, Chenting Wang, Guo Chen, Baoqi Pei, Rongkun Zheng, Jilan Xu, Zun Wang, et al. Internvideo2: Scaling video foundation models for multimodal video understanding. *ArXiv Preprint*, 2024. 2
- [65] Philippe Weinzaepfel, Thomas Lucas, Vincent Leroy, Yohann Cabon, Vaibhav Arora, Romain Brégier, Gabriela Csurka, Leonid Antsfeld, Boris Chidlovskii, and Jérôme Revaud. Croco v2: Improved cross-view completion pre-training for stereo matching and optical flow. In *Proceedings of the IEEE/CVF International Conference on Computer Vision*, pages 17969–17980, 2023. 3
- [66] Bowen Wen, Wenzhao Lian, Kostas Bekris, and Stefan Schaal. You only demonstrate once: Category-level manipulation from single visual demonstration. *rss*, 2022. 2
- [67] Chuan Wen, Xingyu Lin, John So, Kai Chen, Qi Dou, Yang Gao, and Pieter Abbeel. Any-point trajectory modeling for policy learning. *ArXiv Preprint*, 2024. 2, 3
- [68] Yuxi Xiao, Qianqian Wang, Shangzhan Zhang, Nan Xue, Sida Peng, Yujun Shen, and Xiaowei Zhou. SpatialTracker: Tracking any 2D pixels in 3D space. In *IEEE Conference on Computer Vision and Pattern Recognition (CVPR)*, 2024. 3, 8, 1
- [69] Haofei Xu, Jing Zhang, Jianfei Cai, Hamid Rezaatofighi, Fisher Yu, Dacheng Tao, and Andreas Geiger. Unifying flow, stereo and depth estimation. *IEEE Transactions on Pattern Analysis and Machine Intelligence*, 2023. 3
- [70] Mengda Xu, Zhenjia Xu, Yinghao Xu, Cheng Chi, Gordon Wetzstein, Manuela Veloso, and Shuran Song. Flow as the cross-domain manipulation interface. *corl*, 2024. 2
- [71] Gengshan Yang and Deva Ramanan. Upgrading optical flow to 3d scene flow through optical expansion. In *IEEE Conference on Computer Vision and Pattern Recognition (CVPR)*, 2020. 3, 9
- [72] Gengshan Yang and Deva Ramanan. Learning to segment rigid motions from two frames. In *IEEE Conference on Computer Vision and Pattern Recognition (CVPR)*, 2021. 3, 9, 1
- [73] Lihe Yang, Bingyi Kang, Zilong Huang, Xiaogang Xu, Jiashi Feng, and Hengshuang Zhao. Depth Anything: Unleashing the power of large-scale unlabeled data. In *IEEE Conference on Computer Vision and Pattern Recognition (CVPR)*, 2024. 2, 6, 7, 1
- [74] Lihe Yang, Bingyi Kang, Zilong Huang, Zhen Zhao, Xiaogang Xu, Jiashi Feng, and Hengshuang Zhao. Depth Anything V2. *arXiv preprint arXiv:2406.09414*, 2024. 2, 6, 7
- [75] Yao Yao, Zixin Luo, Shiwei Li, Tian Fang, and Long Quan. Mvsnet: Depth inference for unstructured multi-view stereo. In *Proceedings of the European conference on computer vision (ECCV)*, pages 767–783, 2018. 2
- [76] Sijie Zhao, Wenbo Hu, Xiaodong Cun, Yong Zhang, Xiaoyu Li, Zhe Kong, Xiangjun Gao, Muyao Niu, and Ying Shan. StereoCrafter: Diffusion-based generation of long and high-fidelity stereoscopic 3d from monocular videos. *arXiv preprint arXiv:2409.07447*, 2024. 3
- [77] Yang Zheng, Adam W. Harley, Bokui Shen, Gordon Wetzstein, and Leonidas J. Guibas. PointOdyssey: A large-scale synthetic dataset for long-term point tracking. In *IEEE Conference on Computer Vision and Pattern Recognition (CVPR)*, 2023. 6, 1

Supplementary Material

In this supplementary document, we provide comparisons for the inference time, and discuss additional implementation details regarding architecture, dataset and training. Please refer to our project webpage for a high-level overview and video results and comparisons.

1. Inference time

We compare inference time for several approaches we compared against in our paper in Table 1. For a video clip of size $16 \times 224 \times 224$, our inference runs in around 300ms on NVIDIA A6000 to generate output for all the tasks we address in our paper. While our approach does not provide latency low-enough for real-time applications, its inference time of 19ms per-frame makes it at least comparable speed-wise to methods specialized for each task. Our ability to solve multiple perception tasks under a reasonable computational envelope could be potentially useful for many applications like robotics, autonomous vehicles, etc.

2. Training datasets

Our video encoder [58] has been pre-trained on 1.35M video clips across various data sources using masked auto-encoding. To fine-tune our model, we use a limited number of synthetic datasets covering varying a range of annotations, and rely on the priors from the video encoder for generalization.

Kubric [16]. This synthetic dataset has multi-object interactions with many random objects. We use it to generate annotations for depth, flow, motion-based segmentation, and 2D/3D tracking. Each video is 24 frames long, and we use a total of 15k videos from the movi-e and movi-f subsets of the data. Kubric provides meta-data for object and camera trajectories, which could be used to generate 3D tracks. We follow official guidelines and generate the annotations for 3D tracking by sampling around 8-12k tracks in each video. For motion-based segmentation, we use the camera-pose and the 3D track information to detect which 3D tracks come from dynamic vs. static objects, which we then combine with provided rigid-object segmentations to generate annotations for motion-based segmentation.

PointOdyssey [77]. We use this synthetic dataset for depth and 2D/3D tracking annotations. The dataset consists of 159 videos, averaging 2k frames long, with human and object interactions under different lighting and atmospheric conditions. We sample smaller video clips from the long videos to form our dataset.

DynamicReplica [25]. We use this synthetic dataset for depth, flow and 2D/3D tracking annotations. The dataset consists of 524 videos with humans and animals in motion, and we sample smaller video clips to form our dataset.

	Task	GPU	Per-frame time (ms)
RAFT [53]	Optical flow	A100	29
MemFlow [10]	Optical flow	A100	48
DepthAnything [73]	Depth	A100	10
DepthCrafter [20]	Depth	A100	436
RigidMask [72]	Motion Seg.	V100	260
SpaTracker (w/o depth) [68]	3D Track	A6000	17
Ours	All	A6000	19

Table 1. **Inference time.** We compare our per-frame inference time with several task-specific approaches and show at least comparable speed-wise to methods specialized for each task. SpaTracker inference time is measured without the depth estimation.

Since this dataset has higher fps videos, we sample videos with strides of 1, 2 and 4.

TartanAir [62]. Finally, to increase the scene-level data distribution we use TartanAir to generate annotations for flow and depth. The data is collected in photo-realistic simulation environments, with both indoor and outdoor scenes, in the presence of various light and weather conditions. We sample smaller video clips from this dataset.

3. Architecture

Our video encoder [58] processes video-clips of size $16 \times 224 \times 224$. It uses a patch-size of $2 \times 14 \times 14$, which results in $P = 2048$ video tokens, and an embedding dimension of $C = 1408$. It has 40 encoder blocks, and we use output from blocks [14, 21, 28, 36] for DPT heads for dense tasks, while our sparse-head uses features from the last block. We adapt DPT head [41] without any modifications, and only replace 2D-convolutions with 3D. For the sparse head, we adapt two-way attention from SAM [28] without any modifications and following SAM we keep this head lightweight by using only two two-way attention layers. We replace the 2D convolutions in the original mask-decoder of SAM with 3D convolutions. All our input/output tokens are of dimension $C = 1408$ and use learnable embeddings. We use 3D positional encoding for the point query token and the video tokens for the two-way attention stage.

4. Training

We train in two-stages. In the first stage we train all the parameters of our model for depth, flow and 3D tracking on a single window of $T = 16$ frames. During this stage, for each video we estimate all T frames for dense tasks and for 3D tracking we construct a batch of 80 tracks and select point queries randomly across the visible parts of tracks. In the second stage, we further fine-tune our model using unrolled-window training. To train this stage efficiently, we only train for the 2D and 3D tracking tasks and freeze all the parameters, except the last three layers (37-39) of the video encoder and the sparse head. We train on videos of length $S = 40$, windows of size 16 frames and a stride of 8, which results in 4 overlapping windows, and we construct a batch of 48 tracks during this stage, but generate point

queries only in the first 20 frames to force the network to learn long-range tracking. We use AdamW optimizer with a maximum learning rate of 5×10^{-5} and a cosine annealing strategy. Both stages use a batch size of 8, are trained on a single 8-GPU NVIDIA A100 node for 100k iterations and take 1 day and 2 days respectively to train.

For depth, we use SILog [11] loss, for flow, we use L1-loss on the estimated uv-offsets, and for tracking, we use L1-loss for the 2D track positions, scale-invariant loss for the track depth (similar to dense depth), and binary-cross entropy loss for the track visibility. We found the loss weights empirically by first weighting the losses to be in the same order of magnitude and then doing a small hyperparameter search around those weights. We use the loss weights of 20 for the flow and depth losses. For tracking, we use loss weights of 1.0, 20.0, and 15.0 for 2D track position loss, track depth loss and track visibility loss, respectively.